Available online at www.sciencedirect.com

jmr&t Journal of Materials Research and Technology

www.jmrt.com.br

Original Article

Fabrication of nanostructured SnO_2@Co_3O_4/nitrogen doped graphene oxide composite for symmetric and asymmetric storage devices

Sivalingam Ramesh[a], *Hemraj M. Yadav*[b], *Surendra K. Shinde*[c], *C. Bathula*[d], *Young-Jun Lee*[e], *Ravi Kumar Cheedarala*[f], *Hyun-Seok Kim*[d], *Heung Soo Kim*[a,*], *Joo-Hyung Kim*[e,*]

[a] *Department of Mechanical, Robotics and Energy Engineering, Dongguk University –Seoul, Pil-dong, Jung-gu 04620, Seoul, South Korea*
[b] *Department of Energy and Materials Engineering, Dongguk University –Seoul, Pil-dong, Jung-gu 04620, Seoul, South Korea*
[c] *Department of Biological and Environmental Science, Dongguk University-Seoul, Biomedical Campus, Ilsandong-gu, 10326, South Korea*
[d] *Division of Electronics and Electrical Engineering, Dongguk University –Seoul, Seoul 04620, South Korea*
[e] *Department of Mechanical Engineering, Inha University, Incheon, 402-751, South Korea*
[f] *School of Mechanical Engineering, Changwon National University, Changwon, 51140 South Korea*

ARTICLE INFO

Article history:
Received 18 November 2019
Accepted 12 February 2020
Available online 21 February 2020

Keywords:
Ternary composite
Metal oxides
Supercapacitor
Electrochemical properties

ABSTRACT

The fabrication, and characterization of SnO_2@Co_3O_4/NGO composite with a nanogranular-like morphology was synthesized by a thermal reduction process in presence of ammonia and urea as catalyst. The structure and morphology of the composite were investigated by sophisticated techniques. Cyclic voltammetry was performed to determine the electrochemical performance of the composite electrode for supercapacitor applications. The composite symmetrical electrode was displayed a specific capacitance of ~375 F g^{-1} at 0.5 A/g in a 2 M KOH aqueous electrolyte with a capacity retention of ~93% after 10,000 cycles. The SnO_2@Co_3O_4/NGO composite asymmetric electrode exhibited a specific capacitance of~256 F/g at 1 A/g and excellent cyclic retention. The improved electrochemical properties of the composite depends on the nanogranular-like morphology, large surface properties, and excellent conductive networks. Therefore, the ternary oxide@NGO composite electrode is promising architecture for energy storage applications.

* *Corresponding authors.*
E-mails: heungsoo@dgu.edu (H.S. Kim), joohyung.kim@inha.ac.kr (J. Kim).
https://doi.org/10.1016/j.jmrt.2020.02.045

1. Introduction

Recently, the carbon nanotubes, graphene oxide (GO), and porous carbons have attracted significant interest for high-performance supercapacitor applications because of their unique properties such as high electrochemical properties and excellent cyclic stability. Heteroatom-doped carbon materials are widely used electroactive materials owing to their excellent electrochemical performances in supercapacitor applications. Therefore, the carbon-based composite materials are used in portable electronics, hybrid vehicles, and backup energy systems with excellent performances [1–3]. Based on the charge storage mechanism, supercapacitors are mainly categorized as electric double layer capacitors (EDLCs) and pseudo capacitors depending on the materials involved in the electrochemical reaction. Electrodes containing nitrogen-doped graphene oxide (NGO), porous activated carbons, and N-doped carbon source electrode materials are used for supercapacitor applications [4–6]. Redox capacitors or pseudo capacitors such as Co_3O_4, NiO, and MnO_2 and polymer-based electrodes are used for energy storage device applications.

The mainly energy storage materials are depends on the electrostatic interaction increases of charges at the electrode-electrolyte interface via EDLC layer. On the other hand, in pseudo capacitors, the stored energy is released in the presence of reversible redox reactions or faradaic reactions occurring in the metal oxide electrodes [7,8]. The electrochemical performances are enhanced via a control synthesis of mesoporous and microporous carbon materials using a suitable catalyst. The microspores create an effective electrode/electrolyte interface in the EDLCs and provide channels to facilitate electron diffusion [9]. Carbon-based nanostructured materials have attracted great attention because of the outstanding properties of one- and two-dimensional nanotubes and graphene [9–11]. Two-dimensional carbon nanostructure materials have large surface areas and high electronic properties, which enhance the electrochemical properties [12,13]. Different activated carbons and metal oxide materials are used as EDLCs owing to their higher power densities and excellent cyclic stability for supercapacitor applications. NGO materials are thermally stable and biocompatible and have larger surface area of active groups and excellent mechanical properties compared with undoped carbon materials. Nitrogen doping of graphene is carried out by various methods such as substitution reactions and catalytic pyrolysis of organic precursors [14–16]. Based on the n-doping process of carbon materials such as reduced GO can result in a specific capacitance of ~206 F/g and exceptional cyclic stability.

Numerous studies on graphene-based materials have reported an increase in specific capacitance from ~60 F/g at a scan rate of 1 mV/s to 118 F/g at a scan rate of 100 mV/s and 170 F/g at a scan rate of 10 mV/s depending on the electrolyte and electrode materials. Various metal oxide nanoparticles such as Co_3O_4, MnO_2, Fe_3O_4, RuO_2, V_2O_5, and SnO_2 nanoparticles show increased electrical conductivity and specific capacitance with excellent cyclic stability. Recently, a high theoretical capacitance (~3657 F g^{-1}) and excellent stability have been reported for cobalt oxide@carbon electrode materials. Cobalt oxides (Co_3O_4) have been studied as promising candidate electrode materials for supercapacitor applications. Gao et al. reported a Co_3O_4 nanowire on nickel foam that displayed a maximum specific capacitance of ~746 F g^{-1} at a current density of 5 mA cm^{-2} [17–19]. Further, hexagonal Co_3O_4 nanosheets synthesized using complex-precursor materials by a thermal decomposition technique showed a capacitance of ~230 F g^{-1} at 1 A/g with excellent cyclic retention. Nanoporous Co_3O_4 materials synthesized via a hydrothermal process exhibited a capacity of ~280 F g^{-1} with high cyclic stability. Co_3O_4 nanorods synthesized as single crystals for supercapacitor applications showed a maximum capacitance of ~458 F g^{-1} [20]. Co_3O_4 synthesized as an aerogel-like mesoporous material via an addition reaction [21] exhibited a specific capacitance of ~600 F g^{-1} with excellent continuous cycles. Mesoporous Co_3O_4 nanoparticles with a large surface area of ~185 m^2 g^{-1} exhibited a maximum specific capacitance of ~370 F g^{-1} [22]. Besides, tin oxide (SnO_2) is an n-type semiconductor with a wide bandgap of ~3.6 eV and is widely used in the field of solar cells, catalysts, gas sensors, and electrochromic devices. Wang and co-workers studied the microwave-assisted synthesis of SnO_2/graphene, which showed a specific capacitance of ~99.7 F/g and excellent cyclic stability [23]. Li et al. prepared a SnO_2/graphene active electrode by a one-pot synthesis approach; the material showed excellent capacitance and cyclic retention [24]. Velmurugan et al. reported SnO_2/graphene composite [25] electrodes having the combined properties of an EDLC and a pseudo capacitor to enhance the electrochemical properties. As evident from literature [26], nanocomposites synthesized using materials with different morphologies are widely used as electrodes for energy storage applications. Lee et al. [26] synthesized composite nanoparticles of SnO_2 and cobalt oxide by a hydrothermal process. The composite material exhibited an electrochemical capacitance of ~840 F g^{-1} at 10 mV s^{-1} in the potential range of –0.8 V–0.1 V.

Recently, we demonstrated electrochemical supercapacitor applications of binary composite NGO@SnO_2 electrode [27], and it is interesting to investigate the impact of Co_3O_4 nanoparticles incorporation towards electrochemical performance of ternary composite.

Therefore, in the present study, SnO_2@Co_3O_4/NGO porous composite materials were synthesized by a thermal reduction reaction for supercapacitor application using 2 M KOH as an electrolyte. The composite was characterized by field emission transmission electron microscopy (FE-TEM), field emission scanning electron microscopy (FE-SEM), Raman spectroscopy, X-ray diffraction (XRD) analysis, X-ray photoelectron spectroscopy (XPS), and Brunauer–Emmett–Teller (BET) analysis. Furthermore, the electrochemical properties of the SnO_2@Co_3O_4/NGO composite were studied by cyclic voltammetry (CV), galvanostatic charge–discharge (GCD) measurements, and electrochemical impedance spectroscopy (EIS) for supercapacitor application. The SnO_2@Co_3O_4/NGO composite exhibited a high specific capacitance of ~375 F g^{-1} at 0.5 A/g and cyclic stability up to 10,000 cycles, which indicate that the hybrid composite electrode material is promising for supercapacitor application.

2. Experimental

2.1. Materials

In this study, the mandatory chemicals were used in the analytical grade without any purification. Graphene sheet, cobalt nitrate ($Co(NO_3)_2{\cdot}6H_2O$)), tin(IV) chloride ($SnCl_4.5H_2O$), urea (NH_2CONH_2), ammonia, (Sigma–Aldrich, 98%), sulfuric acid (H_2SO_4), potassium hydroxide (KOH), phosphoric acid (H_3PO_4), N-methyl-2-pyrrolidone, potassium permanganate ($KMnO_4$), and polyvinylidene fluoride(PVDF) were acquired from Sigma–Aldrich, South Korea.

2.2. Graphene oxide (GO) synthesis

GO was produced by Hummers' procedure and slightly modified the previous reports of graphite materials [26,28]. Calculated amounts of graphite (6 g), H_2SO_4 (300 ml), H_3PO_4 (40 ml), and $KMnO_4$ (20 g) were mixed in a three-neck flask and heated at 50 °C for 24 h until the formation of graphite sheets. The resultant reaction mixture changed from dark purple to greenish brown, and 30 ml of H_2O_2 solution was added to convert into graphite oxide or graphene oxide. Finally, the GO powder was purified by ethanol and dried in a vacuum oven at 90 °C for 20 h.

2.3. N-doped graphene oxide (NGO) synthesis

A calculated amount of GO (0.6 g) was dispersed in 300 ml of H_2O by ultrasonication for 4 h, which yielded a brownish solution. Then, 50 ml of water was added into the GO suspension and purified by using vacuum oven at 95 °C for 12 h. Then, 1.65 gm of urea and ammonia solution (40 ml) were added to the reaction mixture with continuous stirring for 12 h at 95 °C. Finally, the obtained NGO material was dried in a vacuum oven at 200 °C for 24 h.

2.4. SnO_2@Co_3O_4/NGO composite synthesis via thermal reduction process

In this experiment, calculated amounts of NGO (0.6 g), urea (1.65 g), and ammonia precursor solution (40 ml) were added with continuous stirring at 95 °C for 6 h to form a homogeneous suspension. Then, calculated amounts of 0.01 M $Co(NO_3)_2.6H_2O$ and 0.01 M $SnCl_4.5H_2O$ were dispersed into 300 ml of purified water in a three-neck flask. The reaction was carried out at 95 °C for 12 with continuous stirring, and the entire solution was then transferred to a 300 ml closed autoclave vessel. The reaction product was heated at 200 °C for 12 h and then cooled to room temperature. The product, SnO_2 @Co_3O_4/NGO composite, was further heated at 450 °C for 10 h in a vacuum furnace and purified using water and ethanol. Finally, the SnO_2@Co_3O_4/NGO composite was collected and used for further characterization (Fig. 1).

2.5. Characterization

Raman spectroscopy of the SnO_2 @Co_3O_4/NGO composite was performed using an alpha 300R spectroscope with exceptional speed and sensitivity and high resolution. The crystalloid arrangement of SnO_2@Co_3O_4/NGO was determined by powder XRD analysis (Rotaflex RU-200B, Rigaku) performed using a Cu K_α radiation source. Elemental analysis was carried out by XPS (ESCALAB 250Xi) using Al K_α radiation of 1486.6 eV with an energy source. The morphological analysis of the SnO_2 @Co_3O_4/NGO composite was carried out by FE-SEM (Hitachi S-4800, Japan) and FE-TEM (JEOL, JEM-2010F). BET analysis of the composite sample was performed using an ASAP 2010 analyzer (Micromeritics, USA).

2.6. Fabrication of composite electrodes

The electrochemical properties of the SnO_2@Co_3O_4/NGO composite were determined by mixing 80 wt% composite with 15 wt% carbon black and 5 wt% PVDF in N-methyl-2-pyrrolidone. The composite slurry was then coated on a nickel wire of 1 cm^2 area and dispersed and dehydrated in an oven at 80 °C for 10 h. The quantity of the active electrode was ~1.2 mg. The SnO_2@Co_3O_4/NGO composite was studied using a conventional three-electrode system and a two-electrode arrangement using a CHI 7081C electrochemical workstation. A Ni wire was used to fabricate the composite electrode, while a Pt wire and Ag/AgCl were used as the counter and reference electrodes, respectively. CV experiments were conducted using 2 M KOH as the electrolyte, and EIS was performed in the range of 0.01–105 Hz.

3. Results and discussion

3.1. Fourier transform Raman (FT-Raman) spectral analysis

The FT-Raman spectral analysis was performed to study the NGO materials and their defect structures. Fig. 2(a) and (b) show the Raman spectra of SnO_2@Co_3O_4 and SnO_2@Co_3O_4/NGO composite synthesized by the hydrothermal process. The NGO composite shows a peak at 1579 cm^{-1} corresponding to the G peak of sp^2 C and a D peak at 1342 cm^{-1} that can be ascribed to the breathing modes of the A_{1g} symmetry [29], which indicates the disordered phase of the NGO material. In addition, peaks at 2684–2931 cm^{-1} (2D and 2D') can be seen in Fig. 2(b). The ratio of D and G peak intensities (I_D/I_G) is about ~1.03, which indicates that a large amount of oxygen groups is intercalated between the GO nanosheets via the thermal reduction process [30]. The peaks at 611, 685, 522, and 192 cm^{-1} correspond to the A_1g, A_2u, and B_2g modes of the SnO_2@Co_3O_4/NGO composite, respectively [31].

3.2. Structural analysis by XRD

The structural analysis of graphite, GO, and NGO has been previously reported in literature [32]. The graphite powder showed a characteristic peak at $2\theta = 25.50°$, which corresponds to a GO interlayer spacing of ~0.45 nm. For GO, which was prepared by oxidizing the graphite powder with $KMnO_4$, the peak shifted corresponding to an interlayer spacing of ~0.9 nm, which is characteristic of the GO structure. In addition, the diffraction peak at around $2\theta = 42°$ can be indexed to GO hav-

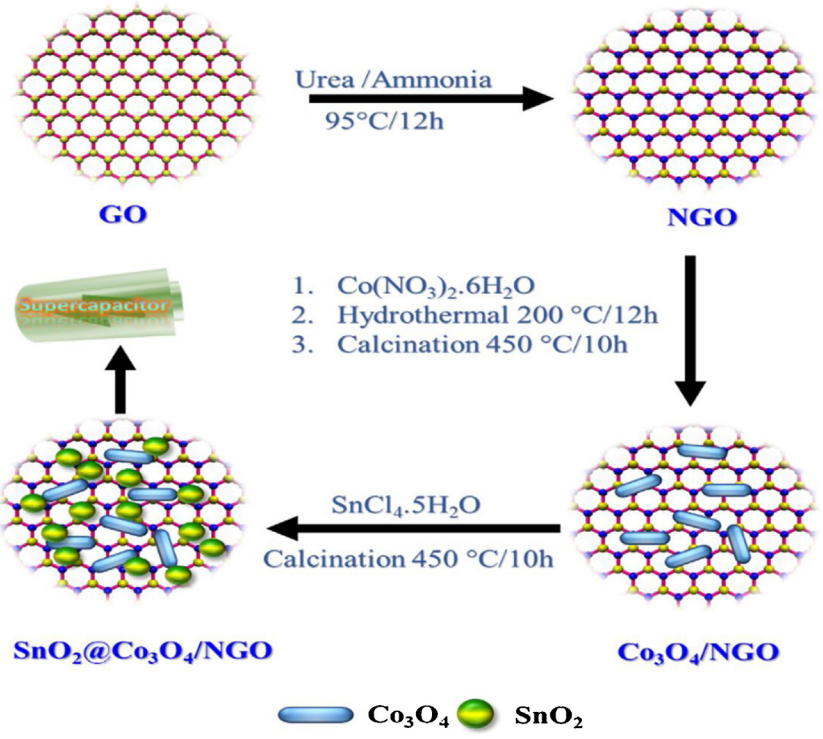

Fig. 1 – Schematic of synthesis of $SnO_2@Co_3O_4$/NGO composite by hydrothermal process.

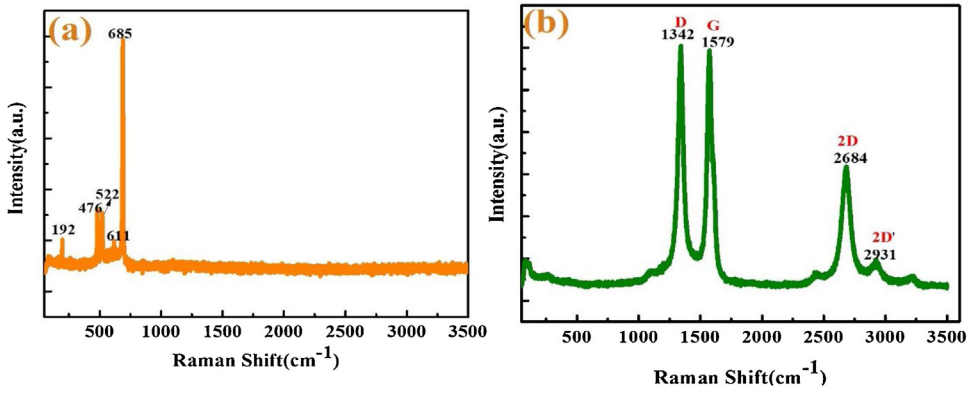

Fig. 2 – (a, b). Raman spectra of (a) $SnO_2@Co_3O_4$ and (b) $SnO_2@Co_3O_4$/NGO composites prepared via thermal reduction process.

ing a turbostratic disorder [33]. The XRD spectra of NGO and the $SnO_2@Co_3O_4$/NGO composite are shown in Fig. 3(a) and (b), respectively. The peaks correspond to the (111), (220), (222), (311), (400), (511), and (440) planes, which can be indexed to the face-centered cubic (FCC) structure of Co_2O_4, as confirmed by standard JCPDS data (card no. 43-1003 and 42-1467). The peaks corresponding to the (110), (101), (200), (211), (220), (310), and (301) planes can be indexed to the tetragonal structure of crystalline SnO_2 in the composite, which matches well with the literature values (JCPDS card no. 41-1445). Therefore, the XRD results prove that the thermal reduction process are shows an important character in the crystalline behaviors confirmed in the previous reports [34].

3.3. *Elemental analysis*

The elemental analysis of NGO and the $SnO_2@Co_3O_4$/NGO composite was performed by XPS. Fig. 4(a–d) show the C 1s (284 eV), O 1s (531 eV), N 1s (395–408 eV), and survey spectra in the range of 0–1400 eV, respectively. The characteristic peaks of N, O, and C atoms are observed in the NGO composite spectra. Fig. 5(a–f) show the XPS profiles of the $SnO_2@Co_3O_4$/NGO composite. The C 1s (284 eV), O 1s (530 eV), N 1s (395–408 eV), and Co 2p and Sn 3d spectra (Fig. 5d, e) confirm the two spin-orbit doublets of cobalt and tin oxides. The Co^{2+} and Co^{3+} peaks appeared at 780 and 795 eV, respectively, while the Sn $3d_{3/2}$ and Sn $3d_{5/2}$ peaks appeared at binding energies of 494 and 486 eV,

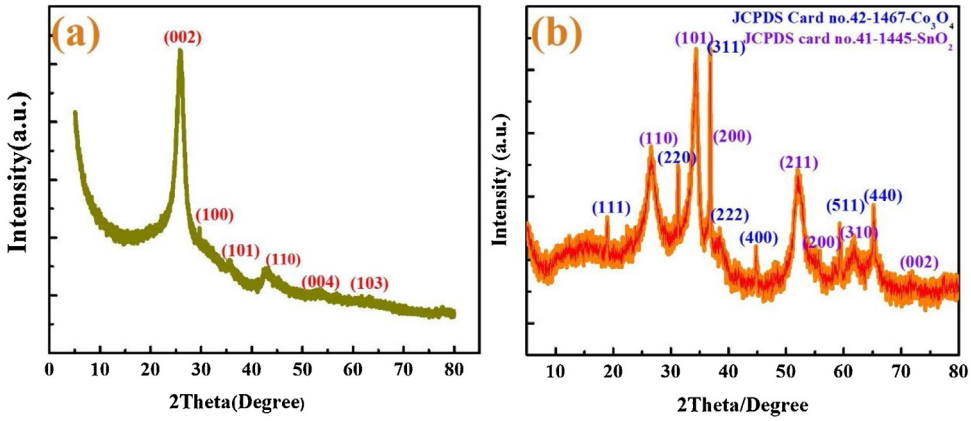

Fig. 3 – (a, b). XRD spectra of (a) NGO and (b) SnO_2@Co_3O_4/NGO composite.

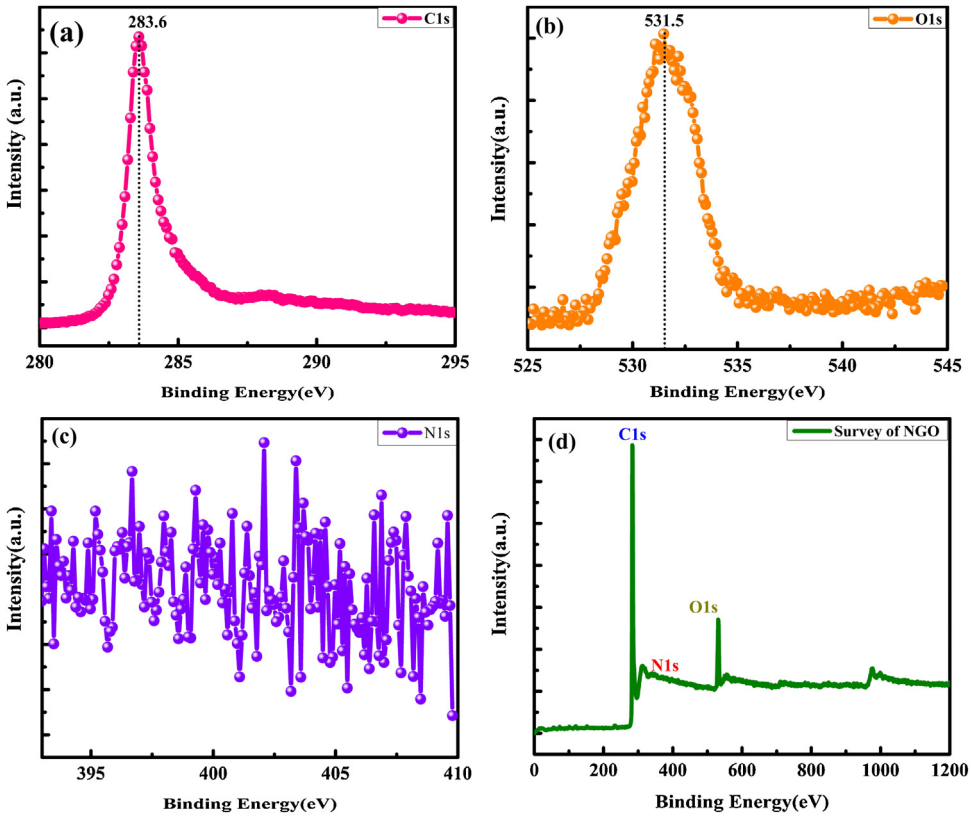

Fig. 4 – (a–d). XPS profiles of (a) C 1s, (b) O 1s, and (c) N 1s, and (d) survey spectrum of NGO composite.

respectively. The XPS survey spectrum (Fig. 5(f)) confirms the presence of C, O, N, Co, and Sn in the composite.

3.4. *Surface morphological properties*

The morphological properties of GO, RGO, and NGO materials and the electrochemical properties of their supercapacitors have been widely studied [35–37]. The morphological properties of the SnO_2@Co_3O_4/NGO composite analyzed by FE-TEM, FE-SEM, and SEM-EDX are presented in Figs. 6–8. The SnO_2@Co_3O_4/NGO composite mainly shows small spherical particles like cauliflower structured and uniformly distributed in the NGO matrix with nanoscale range (~10–30 nm). These nanoparticles are arranged in the larger surface area and shorter diffusion may be provide greater possibility, and excellent rate performance in the active electrode composite material for supercapacitor applications. The SEM-EDX results show the presence of C, O, N, Co, and Sn elements in the hybrid composite (Fig. 7(a,b)).

The HR-TEM images of the hybrid composite show nanocrystalline particles with a size range of ~20–100 nm (Fig. 8(a–f)). The SnO_2@Co_3O_4 nanoparticles with a controlled size in the nanometer scale are well decorated on the NGO matrix. These nanoparticles are arranged as nanorods in the

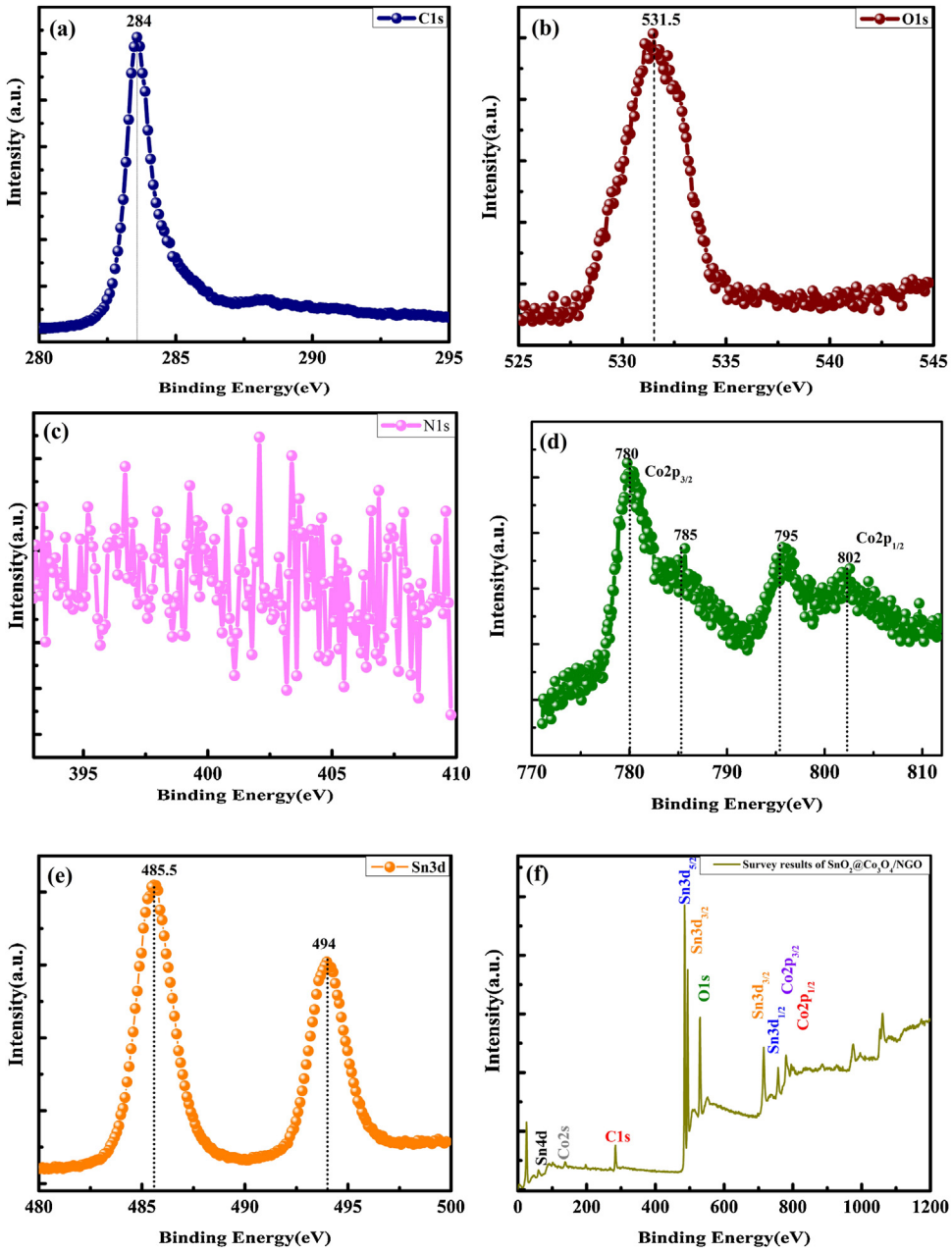

Fig. 5 – (a–f). XPS profiles of (a) C 1s, (b) O 1s, (c) N 1s, (d) Co 2p, and (e) Sn 3d, and (f) survey spectrum of SnO_2@Co_3O_4/NGO composite.

NGO matrix. Fig. 8(d) shows an interlayer spacing of ~0.22 nm, corresponding to the (101) and (311) planes of nanocrystalline SnO_2@Co_3O_4. Therefore, the composite has a conductive core that enhances the remarkable properties in the electrochemical studies. The SAED patterns of the composite (Fig. 8(e,f)) show well-defined rings, which confirm the nanocrystalline structure of SnO_2@ Co_3O_4 in the NGO matrix.

3.5. *Electrochemical properties of SnO_2@Co_3O_4/NGO composite*

GO, RGO, and NGO materials are widely used as electrode materials for energy storage applications [38–40]. The SnO_2@Co_3O_4/NGO composite was used in three- and two-electrode systems with a 2 mol L^{-1} KOH solution as an electrolyte for supercapacitor application. In the present study, CV, GCD measurements, and EIS were performed using a three-electrode system with a strong electrolyte such as 2 M KOH. A Pt wire and Ag/AgCl were used as the counter and reference electrodes, respectively, while the SnO_2@Co_3O_4/NGO composite was used as the working electrode. The electrochemical properties of the composite electrode are shown in Figs. 9 and 10. CV was performed at various scan rates (10–100 mV/s) in the potential range of 0–0.6 V using a 2 M KOH aqueous solution. The CV curves (Figs. 9(a) and 10(a)) display the redox peaks and symmetrical results are indicate that fast

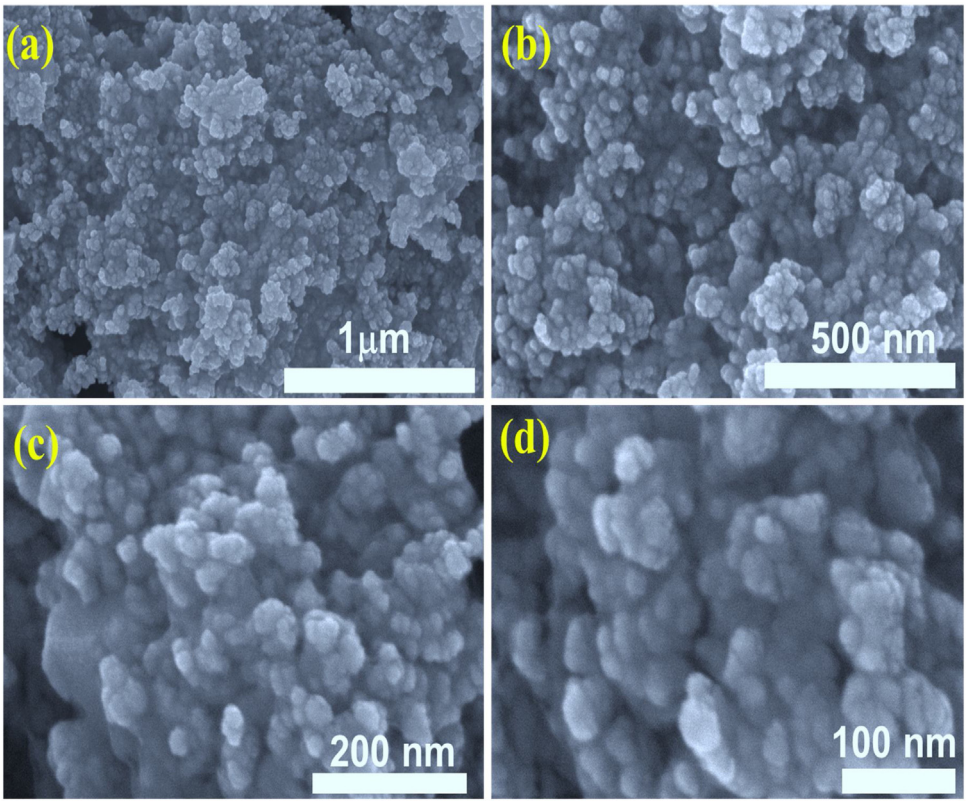

Fig. 6 – (a–d) FE-SEM images of SnO_2@Co_3O_4/NGO composite.

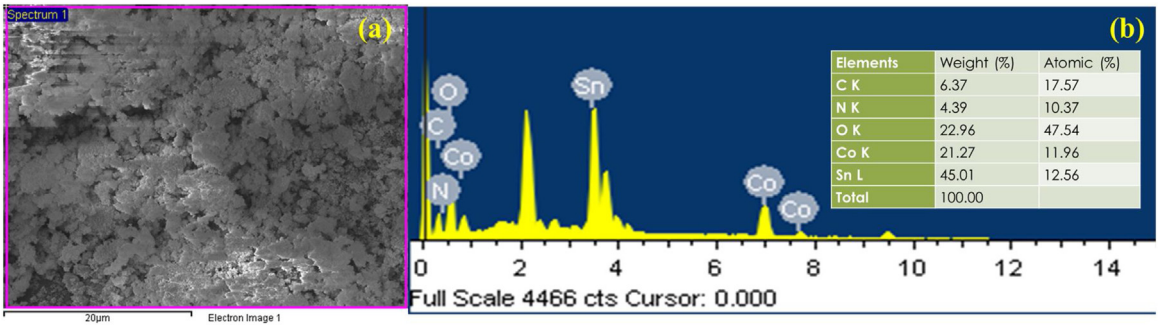

Fig. 7 – (a–b) SEM-EDX results of SnO_2@Co_3O_4/NGO composite.

faradaic reactions and its ideal capacitance, which is possibly due to the enhanced charge–discharge characteristics with a high capacitance at a scan rate of 100 mV/s. The CV curves of the SnO_2@Co_3O_4/NGO composite indicate a redox behavior and EDLC because of the NGO in the presence 2 M KOH solution. The prepared composite appeared to be an ideal electrode material and indicated a pair of redox reactions in the range of 0–0.5 V in the CV curves, which represent the chemical reaction involving the redox process.

$$Co_3O_4 + OH^- \leftrightarrow 3CoOOH + e^- \quad (1)$$

$$CoOOH + OH^- \leftrightarrow CoO_2 + H_2O + e^- \quad (2)$$

In this electrochemical reaction, the anodic peaks represent the positive and negative peaks in the CV curves are due to the redox reactions. This is presumably because the covered Co_3O_4 particles underwent electrochemical charge-transfer reactions in the presence of 2 M KOH electrolyte creation for pseudo capacitor efficient electrode. The previous reports of cobalt oxide materials are strongly recommended the redox couples generally elaborate in the electrochemical system and its redox reactions [38]. Therefore, the non-rectangular CV curves indicate the pseudo capacitance behavior originating from the oxidation-reduction reaction. Furthermore, the CV curves show that with increasing scan rate, the anodic and cathodic peaks shifted toward higher and lower potentials, respectively. The CV curves of the SnO_2@Co_3O_4/NGO com-

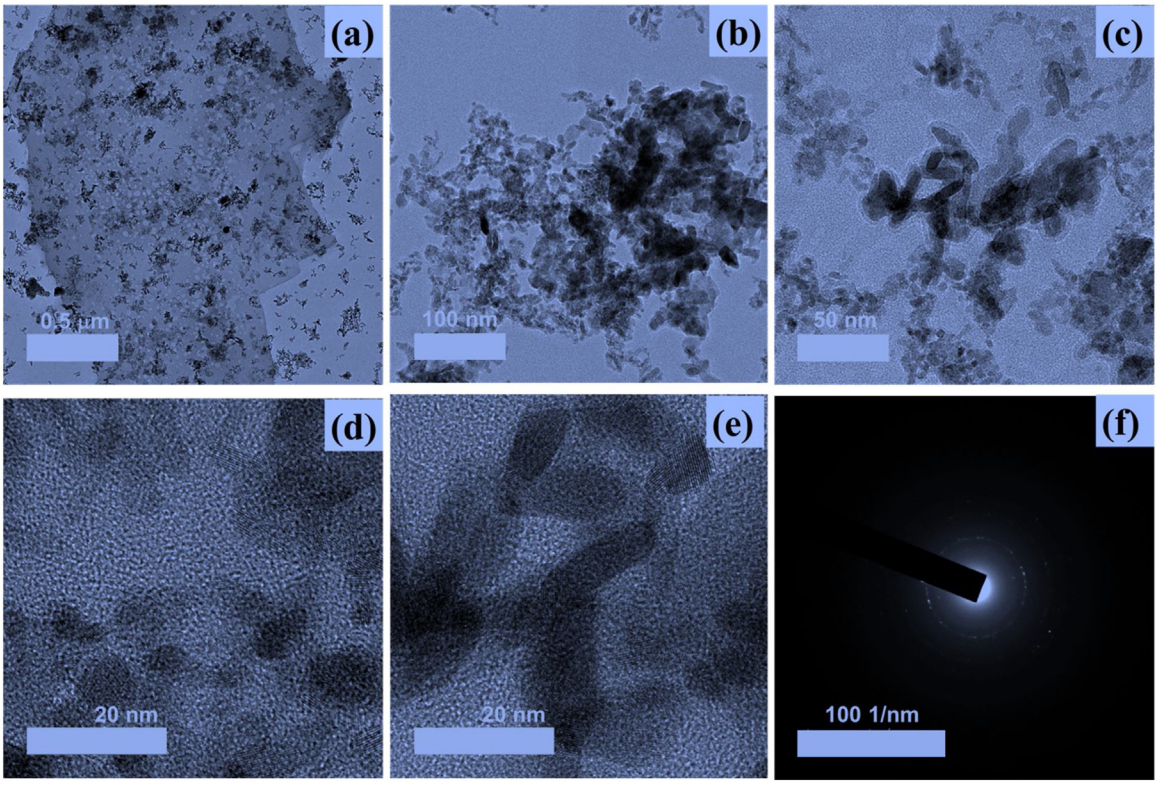

Fig. 8 – (a–f) HR-TEM images of SnO_2@Co_3O_4/NGO composite.

posite indicate a redox reaction between the electrode and electrolyte used in the electrochemical reaction. The CV peaks of the composite electrode to calculate the specific capacitance values of the pristine Co_3O_4 and SnO_2 composite and cyclic stability results were reported in the literature [41]. The storage behavior and energy density of the composite electrode were calculated by the equations [41] reported in previous studies. Figs. 9(b) and 10(b) represent the GCD profiles of the composite electrode at various current densities (0.5, 1, 1.5, 2, 3, and 4 A g^{-1}) using an Ag/AgCl reference electrode. Figs. 9(c) and 10(c) show the specific capacitance of the electrode as a function of current density, which can indicate the electrochemical behavior of the composite. The specific capacitances of the electrode are ~375, 325, 274, 262, and 250 F g^{-1} at current densities of 0.5, 1, 1.5, 2, 3, and 4 A g^{-1}, respectively. The specific capacitance decreased from 375 to 250 F g^{-1} with an increase in current density from 0.5 to 4 A g^{-1}. The specific capacitances of the asymmetric SnO_2@Co_3O_4/NGO electrode are ~255, 186, 148, 126, and 118 F g^{-1} at current densities of 0.5, 1, 1.5, 2, 3, and 4 A g^{-1}, respectively. The capacitance decreased with an increase in current density to 4 A g^{-1} because the electrolyte ions rapidly diffused out of the electrode [42]. This indicates that the electrode performance depends on the active material of the composite electrode. In the present study, the composite electrode was prepared by a thermal reduction process using 0.01 M cobalt nitrate and tin chloride as optimum precursors, with ammonia and urea as the catalysts. The increase in specific capacitance is due to the synergetic effect of SnO_2 and Co_3O_4 in the presence of an NGO network structure. The superior electrochemical performance of the SnO_2@Co_3O_4/NGO material is important for practical supercapacitor application. The substantial improvement in the super capacitive performance and enhanced exploitation of electroactive surface of the composite material than that of pristine cobalt and SnO_2 [43].

EIS was performed using three-electrode symmetric and asymmetric systems with 2 M KOH as an electrolyte. The Nyquist plots show the resistive and capacitive behaviors of the SnO_2@Co_3O_4/NGO composite. In the Nyquist plot, the real axis intercept represents the ESR, contact resistance and the intrinsic things of the composite electrode in the presence the 2 M KOH electrolyte. The ESR and semicircle diameters represent a higher conductivity and lower charge-transfer resistance (R_{ct}) in the low-frequency region, which indicate the high capacitance of the active electrode material. Figs. 9(d) and 10(d) show the EIS profiles of the SnO_2@Co_3O_4/NGO composites. The R_s and R_{ct} indicate an improvement in the electrochemical properties due to the synergetic effect of the metal oxides and NGO. The vertical and the straight sloping R_{ct} confirm the improved capacitive performance of the composite electrodes. The observed semicircles for the composite electrodes indicate faradaic reactions or charge transfer in the active surface of the electrode. The angle between the imaginary and real parts of impedance of the electrode is >45° in the low-frequency region, which implies improved electrochemical properties. The lower ESR values indicate the

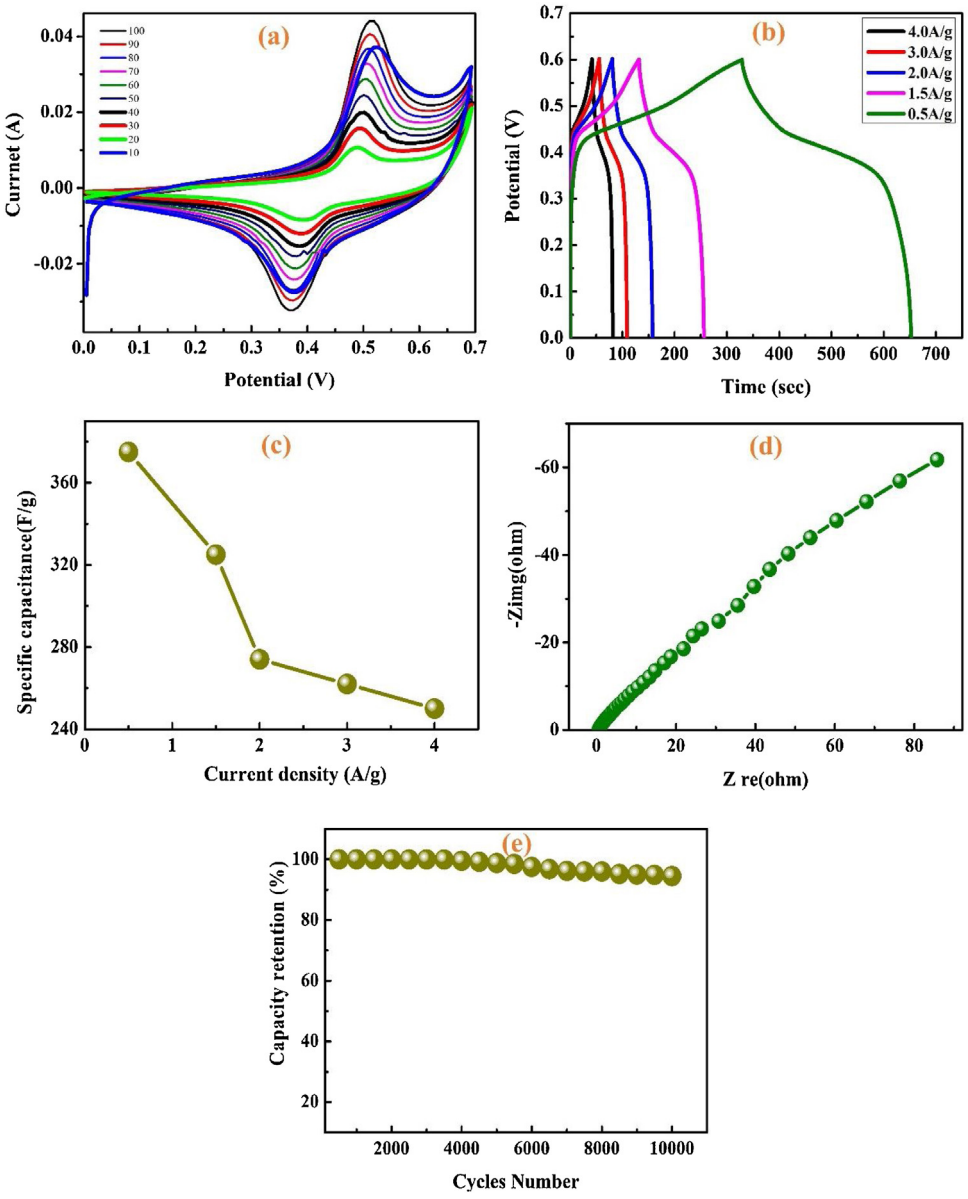

Fig. 9 – (a–e). Electrochemical properties of SnO_2@Co_3O_4/NGO composite electrode: (a) CV profiles, (b) charge–discharge profiles, (c) specific capacitance as a function of current density, (d) EIS spectrum, and (e) capacity retention.

electrochemical behavior of the electrode for supercapacitor application.

Figs. 9(e) and 10(e) show the GCD curves of the composite electrodes for 10,000 cycles at a current density of 0.5 A/g. The results show an improvement in storage capacity during cycling, which indicates the structural commencement and pore opening in the composite material. The specific capacitance of the SnO_2@Co_3O_4/NGO composite remained constant with further charge–discharge cycles and the storage capacity decreased only by ~4.6% after 10,000 charge–discharge cycles at a current density of 0.5 A/g.

4. Conclusions

In this study, a SnO_2@Co_3O_4/NGO composite was synthesized by a thermal reduction process for supercapacitor applications. The storage capacities of the composite electrode were much higher than that of the pristine electrode due to the redox activity of SnO_2@Co_3O_4/NGO. The SnO_2@Co_3O_4/NGO composite symmetrical electrode demonstrated a maximum storage capacity of ~375 F g^{-1} at 0.5 A/g and excellent stability over 10,000 cycles. Therefore, the remarkable structural

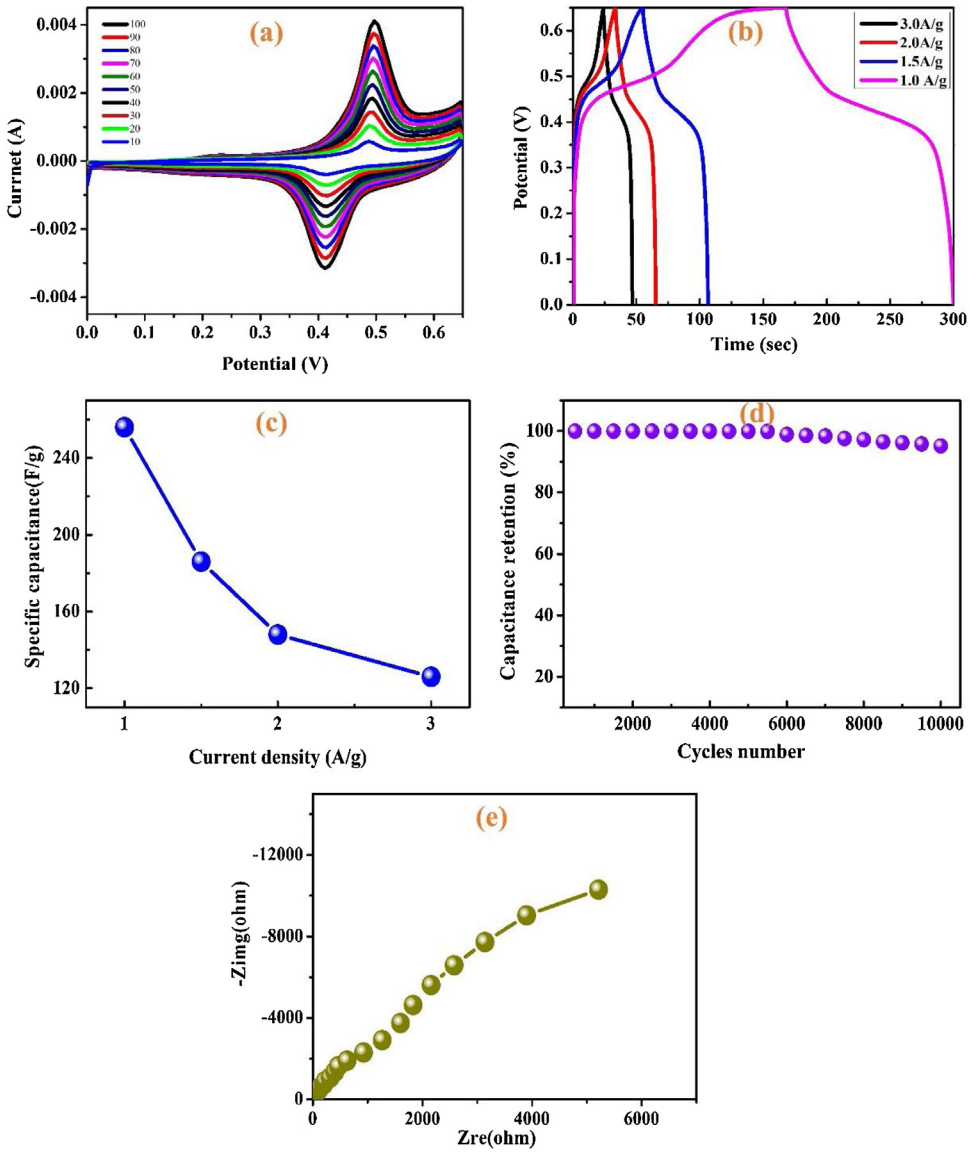

Fig. 10 – (a–e). Electrochemical properties of asymmetric SnO_2@Co_3O_4/NGO composite electrode: (a) CV profiles, (b) charge–discharge profiles, (c) specific capacitance as a function of current density, (d) capacity retention, and (e) EIS spectrum.

and morphological properties and excellent stability (~95% capacity retention) of the composite electrode for promising supercapacitor applications.

Conflict of interest

There is not any conflict of interest.

Acknowledgments

This research programme fully supported by the Basic Science Research Program through the National Research Foundation of Korea (NRF-2017R1D1A1B03028368, funded by the Ministry and Institute for Information & communications Technology Promotion IITP grant funded by the Korea Government MSIP No. R75201600050001002 and Korea Electric Power Corporation Research Institute R16GA02 and supported by the New & Renewable Energy of the Korea Institute of Energy Technology Evaluation and Planning KETEP grant funded by the Korea government Ministry of Knowledge Economy No. 201630 10140550).

Appendix A. Supplementary data

Supplementary material related to this article can be found, in the online version, at doi:https://doi.org/10.1016/j.jmrt.2020.02.045.

REFERENCES

[1] Simon P, Gogotsi Y. Nat Mater 2008;7:845–54.
[2] Salanne M, Rotenberg B, Naoi K, Kaneko K, Taberna P-L, Grey CP, et al. Nat Energy 2016;1:16070.
[3] Brousse T, Bélanger D, Long JW. J Electrochem Soc 2015;162:A5185–9.
[4] Zhu D, Wang Y, Lu W, Zhang H, Song Z, Luo D, et al. Carbon N Y 2017;111:667–74.
[5] Yang W, Yang W, Ding F, Sang L, Ma Z, Shao G. Carbon N Y 2017;111:419–27.
[6] Mondal AK, Kretschmer K, Zhao Y, Liu H, Fan H, Wang G. Microporous Mesoporous Mater 2017;246:72–80.
[7] Thangavel R, Kaliyappan K, Ramasamy HV, Sun X, Lee Y-S. ChemSusChem 2017;10:2805–15.
[8] Li Y, Wang G, Wei T, Fan Z, Yan P. Nano Energy 2016;19:165–75.
[9] Rakhi RB, Chen W, Cha D, Alshareef HN. Nano Lett 2012;12:2559–67.
[10] Wang G, Shen X, Horvat J, Wang B, Liu H, Wexler D, et al. J Phys Chem C 2009;113:4357–61.
[11] Wang L, Liu X, Wang X, Yang X, Lu L. J Mater Sci Mater Electron 2011;22:601–6.
[12] Yang L, Cheng S, Ding Y, Zhu X, Wang ZL, Liu M. Nano Lett 2012;12:321–5.
[13] Andreev AS, Kazakova MA, Ishchenko AV, Selyutin AG, Lapina OB, Kuznetsov VL, et al. Carbon N Y 2017;114:39–49.
[14] Gong K, Du F, Xia Z, Durstock M, Dai L. Science 2009;323:760–4.
[15] Chen S, Bi J, Zhao Y, Yang L, Zhang C, Ma Y, et al. Adv Mater 2012;24:5593–7.
[16] Ramesh S, Karuppasamy K, Yadav HM, Lee J-JJ, Kim H-S, Kim H-S, et al. Sci Rep 2019;9:6034.
[17] Ramesh S, Haldorai Y, Kim HS, Kim J-H. RSC Adv 2017;7:36833–43.
[18] Xiang C, Li M, Zhi M, Manivannan A, Wu N. J Power Sources 2013;226:65–70.
[19] Wang G, Zhang L, Zhang J. Chem Soc Rev 2012;41:797–828.
[20] Farhadi S, Safabakhsh J, Zaringhadam P. J Nanostructure Chem 2013;3:69.
[21] Feng C, Zhang J, He Y, Zhong C, Hu W, Liu L, et al. ACS Nano 2015;9:1730–9.
[22] Xuan L, Chen L, Yang Q, Chen W, Hou X, Jiang Y, et al. J Mater Chem A Mater Energy Sustain 2015;3:17525–33.
[23] Pusawale SN, Deshmukh PR, Lokhande CD. Appl Surf Sci 2011;257:9498–502.
[24] Li F, Song J, Yang H, Gan S, Zhang Q, Han D, et al. Nanotechnology 2009;20:455602.
[25] Yin XM, Li CC, Zhang M, Hao QY, Liu S, Chen LB, et al. J Phys Chem C 2010;114:8084–8.
[26] Wang Yong, Lee Jim Yang, Zeng Hua Chun. Chem Mater 2005;17:3899–903.
[27] Ramesh S, Yadav HM, Lee Y-J, Hong G-W, Kathalingam A, Sivasamy A, et al. Sci Rep 2019;9:12622.
[28] Liu C, Zhao Q. Langmuir 2011;27:9512–9.
[29] Zhao B, Zhang G, Song J, Jiang Y, Zhuang H, Liu P, et al. Electrochim Acta 2011;56:7340–6.
[30] Wang R, Xu C, Sun J, Gao L, Yao H. ACS Appl Mater Interfaces 2014;6:3427–36.
[31] Liu Y, Jiao Y, Yin B, Zhang S, Qu F, Wu X. J Mater Chem A Mater Energy Sustain 2015;3:3676–82.
[32] Duraivel M, Nagappan S, Balamuralitharan B, Selvam S, Karthick SN, Prabakar K, et al. New J Chem 2018;42:11093–101.
[33] Lu T, Zhang Y, Li H, Pan L, Li Y, Sun Z. Electrochim Acta 2010;55:4170–3.
[34] Rakhi RB, Chen W, Hedhili MN, Cha D, Alshareef HN. ACS Appl Mater Interfaces 2014;6:4196–206.
[35] Qorbani M, Naseri N, Moshfegh AZ. ACS Appl Mater Interfaces 2015;7:11172–9.
[36] Xia X, Tu J, Zhang Y, Chen J, Wang X, Gu C, et al. Chem Mater 2012;24:3793–9.
[37] Kung CW, Chen HW, Lin CY, Vittal R, Ho KC. J Power Sources 2012;214:91–9.
[38] Meher SK, Rao GR. J Phys Chem C 2011;115:15646–54.
[39] Dong X-C, Xu H, Wang X-W, Huang Y-X, Chan-Park MB, Zhang H, et al. ACS Nano 2012;6:3206–13.
[40] Ramesh S, Kathalingam A, Karuppasamy K, Kim H-SHS, Kim H-SHS. Compos B Eng 2019;166:74–85.
[41] Ramesh S, Vikraman D, Karuppasamy K, Yadav HM, Sivasamy A, Kim H-SH-S, et al. J Alloys Compd 2019;794:186–94.
[42] Silva R, Pereira GM, Voiry D, Chhowalla M, Asefa T. RSC Adv 2015;5:49385–91.
[43] Zhang G, Wang T, Yu X, Zhang H, Duan H, Lu B. Nano Energy 2013;2:586–94.